Arch Appl Mech (2012) 82:533–556
DOI 10.1007/s00419-011-0571-7

ORIGINAL

Daniel García-Vallejo · Werner Schiehlen

3D-Simulation of human walking by parameter optimization

Received: 9 December 2010 / Accepted: 15 July 2011 / Published online: 7 August 2011

Abstract The simulation of human gait is a complex dynamical problem that requires accounting for energy consumption as well as dealing with a redundantly actuated multibody system. If muscle forces and generalized coordinates are parameterized, optimization techniques allow the simulation of the muscle forces and of the walking motion. An optimization framework is presented for non-symmetrical gait cycles found in the presence of one-sided gait disorders. The motion of each leg is independently parameterized for a whole walking cycle. The non-linear constraints used to fulfill the equations of motion and the kinematical constraints of the different walking phases are implemented in an efficient way. Fifth-order splines are used for the parameterization to reduce the oscillatory behavior coming from non-periodicity conditions. To achieve the computational performance required for three-dimensional simulations, the spline interpolation problem has been split in two parts, one is performed in a preprocessing stage and the other during the optimization. Numerical differentiation via finite differences is avoided by implementing analytical derivatives of the splines functions and of the contractile element force law. The results show good numerical performance, and the computational efficiency for 3D-simulations with one-sided gait disorders is highlighted.

Keywords Parameter optimization · Human walking · Muscle forces · Metabolical energy expenditure

1 Introduction

The simulation of human walking by computer techniques is a major area of research interest for many years. Multibody system dynamics (MSD) techniques are potentially very powerful in this field, and there are many contributions from the MSD community to this challenging problem [3,4,18,20]. The human body can be assumed to be a multibody system actuated by muscles. Even if some researchers have started to study the influence of the deformation of the bones, e.g., Al Nazar et al. [4], it is sufficient to consider that the bones behave as rigid bodies during smooth activities like walking in normal conditions. The human body actuators, the muscles, have their own dynamics that is formulated similar to proportional-integral force actuators. In addition, the alternating contact conditions of the foot on the ground result in a rigid multibody system with a different number of degrees of freedom at each one of the phases of motion. It is expected that the application of the MSD techniques to the problem of human walking will help to understand better how muscles are recruited by the central nervous system (CNS) to move the body in an energy efficient way. This information

D. García-Vallejo (✉)
Department of Mechanical and Materials Engineering, University of Seville,
Camino de los descubrimientos s/n, 41092 Seville, Spain
E-mail: dgvallejo@us.es

W. Schiehlen
Institute of Engineering and Computational Mechanics, University of Stuttgart,
Pfaffenwaldring 9, 70569 Stuttgart, Germany

is important for the design of rehabilitation therapies or surgical interventions and the development of more efficient assistive devices for amputees.

The methods most frequently used to simulate the human walking motion together with the muscle forces responsible for such a motion can be classified into three groups: the so-called *dynamic optimization approach*, the *optimal control approach*, and the *parameter optimization approach*. The dynamic optimization consists of an optimization where the equations of motion of the human body model are integrated forward in time after each iteration of the optimization algorithm for a given set of muscle force histories. The muscle force histories can be expressed in terms of parameters that can be used as design variables of the optimization algorithm. In this kind of methods, the cost function to be optimized is usually a measure of the energy expenditure. One of the most significant contributions to human walking simulation using dynamic optimization is the work of Anderson and Pandy [7]. The main drawback of the dynamic optimization is the high computational cost required due to the many forward integrations of the equations of motion of the human body model. In fact, Anderson and Pandy [7] reported more than 10,000 h of calculation in a computer with 32 processors to achieve a solution for their three-dimensional model. This procedure has also been used to simulate other activities like jumping or pedaling, see Pandy [17].

Transforming the problem into an optimal control problem has provided an efficient method for dynamic simulation of walking. Controllers have been used mainly to preserve the stability of the walker model in forward dynamics simulations. In this regard, Wojtyra [28] used a simple closed-loop control algorithm to stabilize a walking motion by following a measured gait pattern. Peasgood et al. [18] developed a multibody model with a balance controller to dynamically maintain the stability of the model. Then, estimating the metabolical energy cost, an optimization algorithm could be used to find the optimal walking motion of the model.

Parameter optimization techniques have been frequently used for motion synthesis of biped robots [8]. These techniques have been proven to be powerful in two-dimensional human walking simulation as shown by Ackermann [1]. The basics of this approach are the parameterization of the muscle forces and generalized coordinates and the search for their optimal values by minimizing a cost function that includes an energy expenditure estimation and a measure of deviation from normal walking patterns. The method is very much based on the inverse dynamics since at each iteration of the optimization algorithm an inverse dynamic problem is solved by using the motion reconstructed from the optimization parameters. The main advantage of this approach is the complete elimination of the forward integrations of the equations of motion, what significantly reduces the computational cost of simulation. So far, three-dimensional neuromusculoskeletal models of human walking have not been developed in the context of parameter optimization approaches. Recently, Kim et al. [12] used a dynamic motion planning method in which the unknowns are the joint motion time histories of 3D human model. They calculated joint motion histories by minimizing the deviation of the trunk from upright posture as an objective function. However, neural excitations, muscles contraction and activation dynamics, and metabolical expenditure were not considered.

Most of the models of human walking are composed of 7 (2 feet, 2 shanks, 2 thighs, and a pelvis-trunk body) or 8 bodies (2 feet, 2 shanks, 2 thighs, pelvis, and trunk) in which the arms and head are lumped into the trunk by adding its mechanical properties to the trunk body and ignoring their own dynamics. Umberger [24] has studied recently the influence of the arms swing motion on the kinematics, kinetics, and energetics of human walking reporting an influence less than 10%. The high interest in human walking has favored the appearance of specific software for model development. It is worth of mention the work of Delp and Loan [11] who developed a graphic-based software system for developing and analyzing models of musculoskeletal structures.

Planar models have the advantage of being reduced but they can only be used to analyze symmetrical walking motion which makes their applicability very limited. Ackermann [1] used a planar model to analyze the walking motion of humans with bilateral disorders that are in fact much less common than unilateral disorders. When a unilateral disorder is present in the model, the motion is not well represented in the sagittal plane anymore. Therefore, the three-dimensional dynamics is fundamental to properly address the problem of prosthesis design and to understand the influence of disorders in the walking of humans. A very detailed model with 10 bodies and 54 muscles was developed by Anderson and Pandy [7].

This research is devoted to the extension of the parameter optimization approach used by Ackermann [1] to three-dimensional models. This allows one to analyze the sensitivity of the model to the presence of unilateral disorders and to study the human adaptation to this situation. The necessary speed up of the optimization requires the development of advanced methods like the parameterization of the muscle forces and the motion and the muscle contraction and activation dynamics.

This paper is structured as follows. The second chapter presents the multibody model of the human body to be analyzed, including muscle selection issues and details of the contraction and activation dynamics. Section 3 is devoted to the parameter optimization framework used to simulate the three-dimensional motion and muscle forces of the human body model. Finally, some numerical results for one-sided gait disorders are included in Sect. 4.

2 Model description

The human body model used is a three-dimensional rigid multibody system actuated by muscles. The equations of motion of the system are obtained by using the multibody software Neweul-M^2 [13], which generates the equations of motion in symbolic form for efficiently analyzing, simulating and optimizing multibody systems. The skeleton is first considered as an open kinematic chain built from rigid bodies that are connected by holonomic joints and described by a set of n_c generalized coordinates. Thus, starting from the Newton–Euler equations of the rigid bodies in the kinematic chain, the equations of motion are written in terms of the generalized coordinates by virtue of the d'Alembert's principle [21] as

$$\boldsymbol{M}(\boldsymbol{q})\,\ddot{\boldsymbol{q}} + \boldsymbol{k}\left(\boldsymbol{q},\dot{\boldsymbol{q}}\right) = \boldsymbol{q}_r\left(\boldsymbol{q},\dot{\boldsymbol{q}}\right) + \boldsymbol{B}\boldsymbol{A}\boldsymbol{f}^{\boldsymbol{m}} \tag{1}$$

where $\boldsymbol{M}(\boldsymbol{q})$ is the $(n_c \times n_c)$-mass matrix of the system, $\boldsymbol{q}$, $\dot{\boldsymbol{q}}$ and $\ddot{\boldsymbol{q}}$ are the $(n_c \times 1)$-position, velocity and acceleration vectors, respectively. $\boldsymbol{k}$ is a $(n_c \times 1)$-vector describing the generalized Coriolis forces, $\boldsymbol{q}_r$ is a $(n_c \times 1)$-vector including generalized gravitational forces, passive generalized moments at the joints due to tissues interacting with the joints according to the model of Riener and Edrich [19] and generalized viscous damping torques at the knees and hips according to the model of Stein et al. [22], and $\boldsymbol{B}\boldsymbol{A}\boldsymbol{f}^{\boldsymbol{m}}$ is a $(n_c \times 1)$-vector that includes the generalized forces exerted by the muscles actuating the model. The $(N_m \times 1)$-vector $\boldsymbol{f}^{\boldsymbol{m}}$ summarizes the forces generated by a reduced set of N_m muscles included in the model as described in Appendix A. Matrix $\boldsymbol{A}$ is the constant $(n_b \times N_m)$-matrix of moment arms and is used to calculate the torques generated by all muscles at the actuated joints, where n_b is the number of actuated joints, and matrix $\boldsymbol{B}$ is a $(n_c \times n_b)$-distribution matrix used to obtain the generalized torques due to the torques at the actuated joints.

The three-dimensional model of the human body used in this research is composed of 7 rigid bodies, two thighs, two shanks, two feet, and a body called HAT representing the pelvis, trunk, arms, and head, which are connected by holonomic joints, see Fig. 1. The thighs are connected at the hips to the HAT by spherical joints,

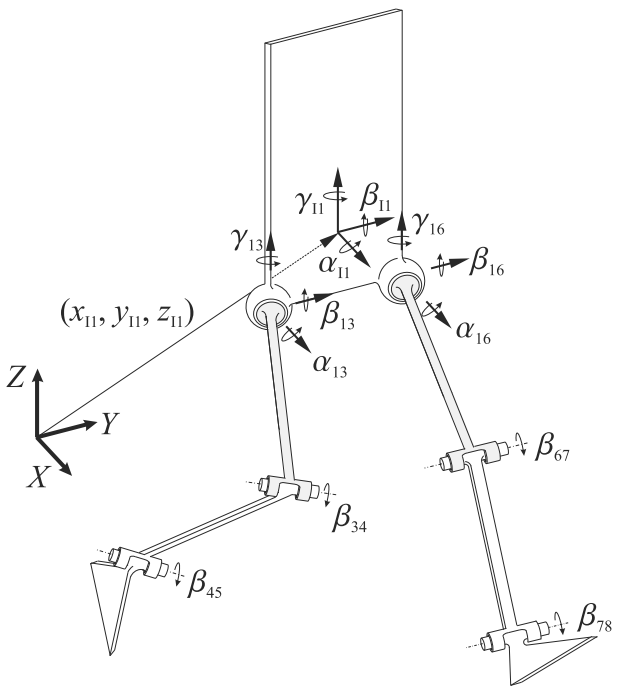

Fig. 1 Model of the human body

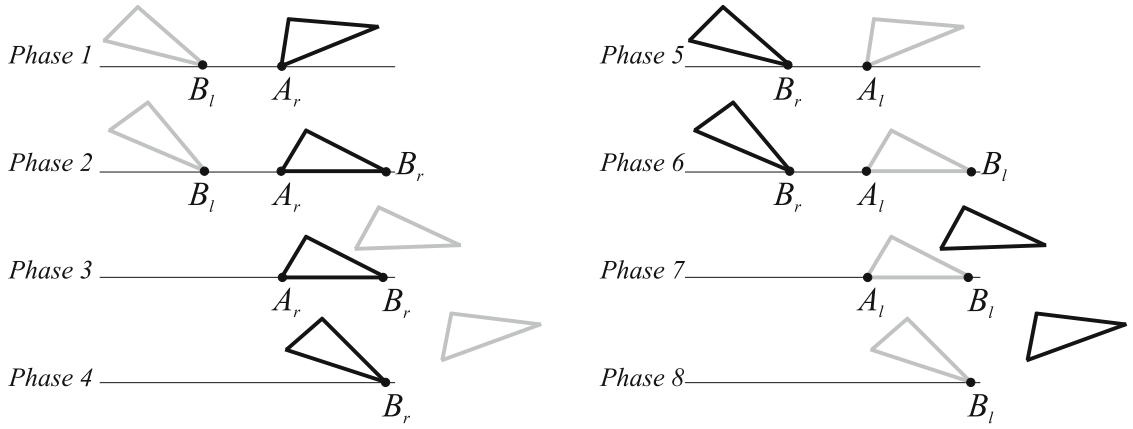

Fig. 2 Sketch of the contact conditions

the shanks and thighs are connected by revolute joints representing the knees, and the foot and shanks are connected by revolute joints representing the ankles. This is a simplification of other three-dimensional models that can be found in Anderson and Pandy [6]. However, this simplification allows the derivation by software Neweul-M^2 of the equations of motion of the tree composed by the mentioned 7 bodies without any constraint. This simple model is used to study the proposed optimization framework in a three-dimensional simulation. More realistic results could be obtained by using a more general representation of the joints, specially of the ankle joints. For a more detailed description of the knee and ankle joints see Zatsiorsky [29].

The kinematic chain in Fig. 1 is described by the following vector of 16 generalized coordinates

$$\boldsymbol{q} = \left[x_{I1}\ y_{I1}\ z_{I1}\ \alpha_{I1}\ \beta_{I1}\ \gamma_{I1}\ \alpha_{13}\ \beta_{13}\ \gamma_{13}\ \beta_{34}\ \beta_{45}\ \alpha_{16}\ \beta_{16}\ \gamma_{16}\ \beta_{67}\ \beta_{78}\right]^T \tag{2}$$

where the subscript I refers to the inertial frame, subscript 1 refers to body HAT, which is in composed of the pelvis and the trunk, subscripts 3 and 6 refer to right and left thighs, respectively, subscripts 4 and 7 refer to right and left shanks, respectively, and subscripts 5 and 8 refer to right and left feet, respectively. When a subscript is written as ij, it means a relative motion of body j with respect to body i. It shall be noted here that Neweul-M^2 is programmed based on the most common sequence of rotation 123, while in Biomechanics the sequence 213 is usually considered anatomically meaningful, Zatsiorsky [29] and Allard, Cappozzo et al. [5]. However, while the spatial rotations of the members are the same using the different rotation sequences, for comparison with other authors' results, the 213 sequence has been used.

Once the kinematic chain representing the skeleton is described, the contact of this chain with the ground is added. The contact conditions in the different walking phases are represented by unilateral constraints. However, due to the use of an optimization framework in which it is possible to constrain the normal contact forces to be only positive, the contact with the ground is modeled using simple bilateral constraints associated with the joints attached to the feet. Therefore, the contact forces can be easily added to the model by using a vector of Lagrange multipliers as

$$\boldsymbol{M}\left(\boldsymbol{q}\right)\ddot{\boldsymbol{q}} + \boldsymbol{k}\left(\boldsymbol{q},\dot{\boldsymbol{q}}\right) = \boldsymbol{q}_r\left(\boldsymbol{q},\dot{\boldsymbol{q}}\right) + \boldsymbol{B}\boldsymbol{A}\boldsymbol{f}^{\boldsymbol{m}} + \boldsymbol{C}_{ph}^T\boldsymbol{\lambda}_{ph} \quad (ph = 1, 2, \ldots, 8) \tag{3}$$

where $\boldsymbol{\lambda}_{ph}$ is the vector of Lagrange multipliers at phase ph of the motion. Note that the previous equation is used together with constraints equations forcing the normal contact forces to be always positive. Moreover, hard impacts will be avoided.

The contact conditions of different phases of the walking cycle are summarized in Fig. 2 in agreement with the model of the foot adopted. Note that A_r and B_r are used to refer to the right heel and right toe, respectively, while A_l and B_l are used to refer to the left heel and left toe, respectively.

In the formulation of contact, it is assumed that there is no sliding of the feet during the whole cycle of walking. The contact conditions at the different phases are modeled as follows:.

- *Phase 1*: the left toe contact is modeled by constraining the three displacements of point B_l and the rotation of the foot around an axis perpendicular to the flat surface of the ground (pivoting). On another hand, the right heel contact is modeled by constraining the three displacements of point A_r and the rotation of the foot around an axis perpendicular to the flat surface of the ground.

- *Phase 2*: due to the contact of the right toe, a constraint to the vertical displacement of point B_r is added to the constraint set of phase 1.
- *Phase 3*: the contact at the left toe is removed.
- *Phase 4*: the contact at the right heel is also removed. The right toe contact is modeled by constraining the three displacements of point B_r and the pivoting rotation of the foot around an axis perpendicular to the ground.
- *Phase 5*: the left heel gets in contact with the ground and this contact is modeled by constraining the three displacements of point A_l and the pivoting rotation of the foot around an axis perpendicular to the ground.
- *Phase 6*: due to the contact of the left toe, a constraint to the vertical displacement of point B_l is added to the constraint set of phase 5.
- *Phase 7*: the contact at the right toe is removed.
- *Phase 8*: the contact at the left heel is also removed. The left toe contact is modeled by constraining the three displacements of point B_l and the pivoting rotation of the foot around an axis perpendicular to the ground.

2.1 Muscles actuating the multibody model

The muscle groups selected for this research are based on the work of Anderson and Pandy [6]. These authors developed a three-dimensional model for vertical jumping which can also be used for walking analysis since walking is a less demanding activity. It is also expected that the set of muscles used by these authors could be reduced, since some of them may show a low enough activation during walking. Such a low activation would result in a small muscle torque at the joints the muscle spans.

There is a need for selecting a criterion that allows one to combine muscles in groups. The first idea to keep in mind is that the muscles to be included in the same group must have the same main function. Then, averaged values of the moment arms will be obtained. This has been done previously by other authors, for instance, Menegaldo et al. [14] suggested to obtain averaged values of certain muscle properties by using as weights the products of the maximum force by the moment arm about each joint of the different muscles that are to be combined. This criterion gives more importance to the muscles in the group that may produce a larger joint moment during walking. Then, it is required to have the values of the forces exerted by each muscle during a cycle of walking. To that end, the results obtained by Brand et al. [9] are used. In Ref. [9], the authors obtained the peak force of each one of the musculotendon actuators during a walking cycle of normal gait. With the peak forces, peak joint moments can be obtained and used as a measure of the contribution of each muscle to the motion. This criterion is used in this investigation to average the moment arms for each muscle group from the moment arms calculated by Menegaldo [15].

The previous idea can also be used to neglect certain muscles from the ones used by Anderson and Pandy [6] so that the muscle set can be further reduced for the sake of simplicity. In order to check the contribution to gait of each one of the muscle groups, the product of the averaged moment arm by the maximum force of the muscle obtained by Brand et al. [9] can be used. These products are the maximum values of the moment components corresponding to each muscle group during a walking cycle. Then, comparing the resultant moments one to each other, it is concluded which are the muscles or muscle groups that can be neglected. Table 1 contains the values of the muscle torques contributed by each muscle or muscle group. The names in bold are the muscles or muscle groups that are neglected due to their small contribution to walking.

2.2 Inversion of activation and contraction dynamics

An important part of the optimization process used to simulate a walking cycle is the inversion of the contraction and activation dynamics, see Ackermann [1]. The inversion of the contraction dynamics is needed to obtain the values of the muscle activation, a, since they are required to evaluate the energy expenditure according to the procedure proposed by Umberger et al. [25]. Once the activations are obtained, using their time derivative, $\dot{a}$, it is possible to invert also the activation dynamics so that the neural excitations, u, are also obtained, see Appendix C. The neural excitations are required for two reasons: one is that they are also involved in the calculation of the muscle energy expenditure and the other is that they are involved in some of the non-linear constraints of the optimization procedure since their values must lay in the interval [0, 1].

In the work of Ackermann [1], the muscle forces are parameterized by using cubic splines, which have C^2 continuity. The values of the muscle forces at certain time nodes are included in the set of optimization

Table 1 Analysis of the different muscle group contributions to motion

Muscle	M_h^{peak} (Nm)	$\frac{M_h^{\text{peak}}}{M_h^{\max}}$ (%)	M_k^{peak} (Nm)	$\frac{M_k^{\text{peak}}}{M_k^{\max}}$ (%)	M_a^{peak} (Nm)	$\frac{M_a^{\text{peak}}}{M_a^{\max}}$ (%)
SOL	0	0	0	0	159.85	100
TA	0	0	0	0	37.11	23.22
GAS	0	0	33.02	11.19	87.5	54.74
BFSH	0	0	26	**8.81**	0	0
VAS	0	0	295.2	100	0	0
RF	60.19	42.15	50.46	17.09	0	0
HAMS	142.8	100	117.23	39.71	0	0
GRA	14.67	**10.28**	5.18	**1.76**	0	0
TFL	18.16	12.72	0	0	0	0
SAR	13.98	**9.79**	2.47	**0.84**	0	0
GMAXL	81.64	57.17	0	0	0	0
GMAXM	39.55	27.69	0	0	0	0
GMEDA	61.8	43.28	0	0	0	0
GMEDP	50.43	35.31	0	0	0	0
ADM	86.19	60.35	0	0	0	0
ADLB	69.97	49	0	0	0	0
ILPSO	55.65	38.97	0	0	0	0
PECT	13.94	**9.76**	0	0	0	0
PIRI	15.32	**10.73**	0	0	0	0

Bolded names correspond to muscles contributing with less than a 10% of the maximal contribution. The moment components M_h, M_k, and M_a are related to hip, knee, and ankle, respectively

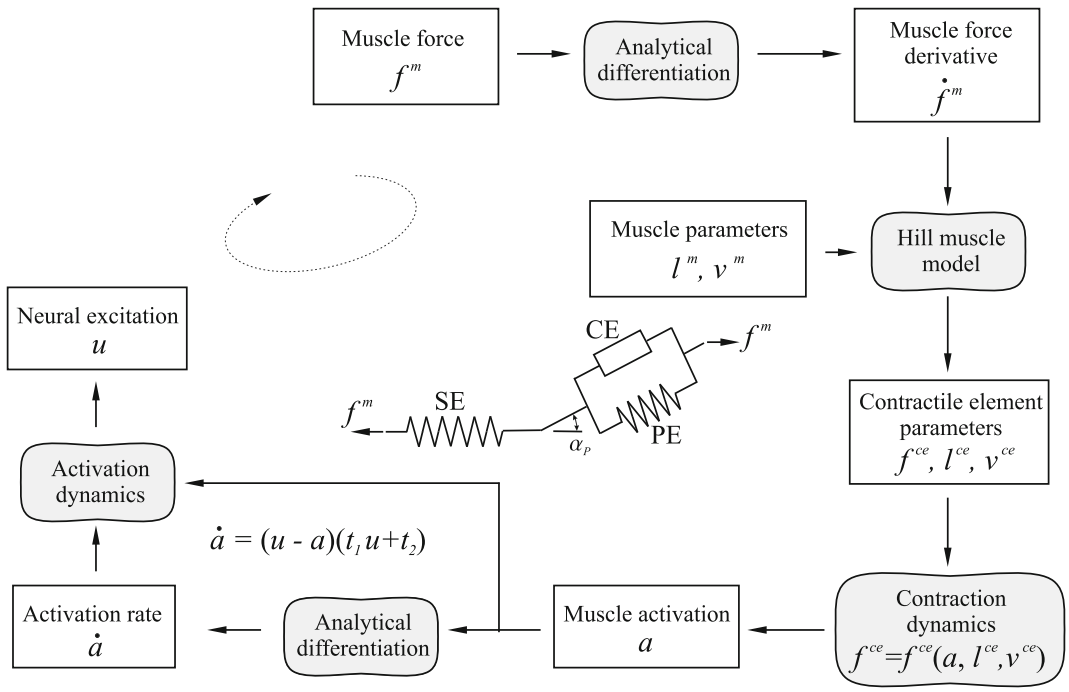

Fig. 3 Flow diagram of the inversion of the activation and contraction dynamics

variables. Then using numerical differentiation, the time derivative of the muscle force at another set of points, the so-called control points, is computed by centered finite divided differences and other numerical formulae obtained from truncated Taylor series. Since the control points are not uniformly distributed along the gait cycle, the use of the previously mentioned numerical differentiation formulae leads to a non-uniform distribution of the accuracy of the time derivative along the gait cycle.

The calculation of the time derivative of the muscle force is carried out by implementing the analytical derivative of an higher order spline polynomial in the interpolation subroutine. Furthermore, the time derivative of the activation, what is required when inverting the activation dynamics, can also be obtained after some calculations due to the implementation of the first and second derivatives of the spline polynomials. Figure 3 shows a flow diagram summarizing the inversion process of the contraction and activation dynamics.

3 Parameter optimization

The simulation of human walking motion is now treated as a huge parameter optimization problem. The optimization parameters, also called design variables, are used to reconstruct the muscle force histories and the generalized coordinate histories of a walking cycle as well. Such a set of parameters is found by minimizing a cost function which is evaluated based on the energetic and esthetic reasons. Finally, the motion and muscle forces time histories reconstructed from the optimization parameters are asked to fulfill many constraints. The constraints of the constrained optimization problem ensure the fulfillment of the equations of motion of the multibody system, the kinematic constraints as well as other physical and physiological relations.

The complete set of design variables is summarized in vector $\boldsymbol{\chi}$. This vector is itself built from four different vectors as follows:

1. A vector $\boldsymbol{q}_i, i = 1, 2, \ldots, n_c$, containing all nodal values of the different generalized coordinates.
2. A vector $\boldsymbol{f}^m_j, j = 1, 2, \ldots, N_m$, containing all nodal values of the different muscle forces. Since each muscle force is parameterized as the generalized coordinates are, a similar number of design variables can arise from muscle forces.
3. A vector with eight components representing the durations of the eight phases of a walking cycle $\boldsymbol{t}_{ph}$.
4. A vector with geometrical parameters describing the kinematic constraints of the feet on the ground $\boldsymbol{p}_g$.

According to the previous explanation, the vector of design variables can be written as:

$$\boldsymbol{\chi} = \left[\boldsymbol{q}_1^T, \ldots, \boldsymbol{q}_{n_c}^T, \ldots, \boldsymbol{f}_1^{mT}, \ldots, \boldsymbol{f}_{N_m}^{m\ T}, \ldots, \boldsymbol{t}_{ph}^T,\ \boldsymbol{p}_g^T\right]^T \tag{4}$$

with

$$\begin{aligned} \boldsymbol{t}_{ph} &= [t_1,\ t_2, \ldots, t_8]^T \\ \boldsymbol{p}_g &= [L_R,\ L_L,\ \alpha_R,\ \alpha_L,\ L_W]^T \end{aligned} \tag{5}$$

where L_R and L_L are the right and left step lengths, α_R and α_L are the right and left orientation angles of the feet, and L_W is the lateral distance between both ankles.

3.1 Optimization framework

Minimizing energy expenditure during walking is a reasonable criterion that the central nervous system uses when dealing with muscles recruitment, specially when walking long distances. For this reason, it makes sense to obtain muscle forces and generalized coordinates by minimizing the metabolical cost of walking. In this investigation, the energy expenditure model due to Umberger et al. [25] is used as measure of the metabolical cost. This energy measure was also used by Ackermann [1] while other authors have used different cost functions as for example a measure of the muscle fatigue, see Brand et al. [9] and Peasgood et al. [18].

Umberger et al. [25] provided a measure of the metabolical expenditure including thermal and mechanical energy liberation rates during simulated muscle contractions of mammalians at normal body temperature. According to their model, the total energy rate of a single muscle is written as follows:

$$\dot{E} = \dot{E}\left(l^{\mathrm{ce}}, v^{\mathrm{ce}}, f^{\mathrm{ce}}, a, u, \boldsymbol{p}\right) \tag{6}$$

where l^{ce} is the contractile element length, v^{ce} is the contractile element velocity, f^{ce} is the contractile element force, a is the muscle activation, u is the neural excitation, and $\boldsymbol{p}$ is a vector summarizing all muscle constant parameters required to evaluate the energy rate, see Umberger et al. [25]. The previous expression of the energy rate can be integrated in time in order to obtain the amount of energy spent during walking as

$$E = \int_{t_0}^{t_f} \dot{E}\left(l^{\mathrm{ce}}, v^{\mathrm{ce}}, f^{\mathrm{ce}}, a, u, \boldsymbol{p}\right)\mathrm{d}t \tag{7}$$

A more meaningful measure of energy consumption when considering walking long distances in normal conditions is the energy expended per unit of length what can be obtained by dividing the total energy of one cycle by the distance walked. This is called the total energy of transportation and reads as

$$E^t = \frac{E}{L_R + L_L} \tag{8}$$

where L_R and L_L are the right and the left steps walked in the simulated cycle.

Since the time histories of the muscle forces and of the generalized coordinates are obtained by optimization techniques trying to minimize the energy consumption, there is a need to follow a certain motion pattern. Otherwise, in an attempt to reduce the energy expenditure, a non-logical solution could be found. For example, standing in equilibrium in vertical position without muscle contraction seems to be a low energy configuration. Therefore, a measured walking motion is used to force the model to follow a certain motion. This fact has some other advantages in the case of designing prosthesis. One of these advantages is that the simulated motion of an individual wearing a prosthesis will be close to normal walking patterns which is desirable for esthetical reasons. Another advantage is related with the contact forces at the feet. The simulated contact forces will be close to those of a normal walking cycle what would result in no significant modification of the contact forces at the non-damaged foot. This is reasonable in case of non-severe damages since other aspects like pain may be more important than enforcing a symmetric walking motion.

The deviation with respect to normal walking patterns is evaluated as follows:

$$J_{\text{dev}} = \int_{t_0}^{t_f} \sum_{i=1}^{n_x} \frac{\left(x_i\,(t) - x_i^m\,(t)\right)^2}{\sigma_i^2} \mathrm{d}t \tag{9}$$

where x_i is a time-dependent variable of the model and x_i^m refers to the experimentally measured value of the same variable. These variables, x_i with $i = 1,\ 2, \ldots, n_x$, include the generalized coordinates and ground reaction forces. In (9), σ_i is a characteristic measure of the time variability of x_i. Dividing by σ_i the differences between measured and simulated values of all x_i are scaled. In the work of Ackermann [1], the standard deviation obtained by measuring the walking motion of many subjects and provided by Winters [27] was used as σ_i. Since in this investigation, not a mean walking motion but the walking motion of one particular subject is used, a measure related to the motion used is preferred. Therefore, the mean square deviation with respect to the averaged mean is used as a measure of the time variability as

$$\sigma_i = \frac{1}{T}\sqrt{\int_{t_0}^{t_f} (x_i\,(t) - X_i)^2 \mathrm{d}t} \quad \text{with} \quad X_i = \frac{1}{T}\int_{t_0}^{t_f} x_i\,(t)\mathrm{d}t. \tag{10}$$

where X_i is the average of $x_i\,(t)$ in the measured walking cycle. The measured motion used in this research was obtained by Ackermann and Gros [2] by measuring the walking motion of a subject wearing sport shoes and walking at his preferred velocity.

Due to skin artifacts, some errors in the measured motion occur. Such errors are probably of different significance for each generalized coordinate but it seems to be logical that errors due to skin artifacts are relatively more significant for those generalized coordinates that experience a smaller time variation. For instance, the generalized coordinate describing the flexion-extension of a leg may vary with $\sigma = 0.35$, while the generalized coordinate describing femur rotation may vary only with $\sigma = 0.03$ during the measured cycle, what means that femur rotation is not very significant during normal walking. Due to the measured rotation may be more contaminated by the skin artifact errors and it makes sense to give more importance to better captured motion by introducing weighting factors in Eq. (9) as

$$J_{\text{dev}} = \int_{t_0}^{t_f} \sum_{i=1}^{n_x} \omega_i \frac{\left(x_i\,(t) - x_i^m\,(t)\right)^2}{\sigma_i^2} \mathrm{d}t \tag{11}$$

In this investigation, weighting factors have been calculated as

$$\omega_i = \sigma_i \,/\sigma_i^{\max} \tag{12}$$

being $\sigma_i^{\max}$ the maximum σ_i $(i = 1, 2, \ldots)$. Notice that due to the much larger variability of the ground reaction forces, the weighting factors for generalized coordinates are calculated with their corresponding $\sigma_i^{\max}$.

Finally, the value of the cost function is calculated using the the metabolical cost of transportation, E^t, and the measure of the deviation from normal walking patterns, J_{dev}, as follows:

$$f = \omega_E \frac{E^t}{100} + \omega_J J_{\text{dev}}, \tag{13}$$

where E^t is divided by the factor 100 to obtain a value with the same order of magnitude of J_{dev} for balancing of the two terms of the cost function (13) to get comparable numbers, and ω_E and ω_J are two weighting factors.

3.2 Parameterization

The procedure suggested by Ackermann [1] and used in this research avoids the forward integration through parameterization of the time histories of the generalized coordinates by using spline polynomials and by searching for their optimum values at certain node positions. Since walking is a periodic motion, other authors have also used Fourier series to parameterize the motion, i.e., Peasgood et al. [18]. Spline functions have many possibilities that can be used to improve the efficiency of the procedure. In fact, it is easy to have access to the derivatives of the parameterized function, avoiding the numerical differentiation used by Ackermann [1]. In addition, the interpolation can be split into two parts: a more computationally expensive one that can be done in a pre-processing stage and the other that is done during the optimization.

As explained by Ackermann [1] and Bessonnet et al. [8], in order to avoid jerky variations of moments at the joints, generalized coordinates must be approximated by using C^3 splines, at least. This, in general, would lead to solve a linear system of equations of size $5n - 5$, being n the number of nodes used to approximate. However, it is possible to reduce the size of the interpolation problem by algebraic manipulations previous to the solution of the linear systems. In this work, fifth-order splines with periodic boundary conditions are used to parameterize muscle forces and generalized coordinates.

It is observed that when periodic boundary conditions are used to obtain the interpolating spline polynomials from a set of points which are not fully periodical in terms of the function values and their derivatives, an oscillating behavior is induced into the spline polynomials. This undesirable oscillating behavior may hamper the convergence of the optimization algorithm. The reasons for this lack of periodicity are twofold. On the one hand, the measured motion that is used as a normal walking pattern and serves as the basis to evaluate the deviation from normal walking patterns is not perfectly periodic. The attempt to minimize such a deviation transfers the mentioned non-periodic behavior to the muscle forces and generalized coordinates. On another hand, during the iterations of the optimization algorithm, any partial result may admit a certain degree of non-periodicity due to numerical reasons. In this research, the above mentioned oscillatory behavior is decreased by forcing the periodicity of the set of points used to calculate the interpolating polynomials. In the case of fifth-order periodical splines, the degree of periodicity is defined according to

$$\begin{aligned} f_1 &= f_N \\ f_1' + O\left(h^3\right) &= f_N' + O\left(h^3\right) \\ f_1'' + O\left(h^3\right) &= f_N'' + O\left(h^3\right) \\ f_1''' + O\left(h^3\right) &= f_N''' + O\left(h^3\right) \end{aligned} \tag{14}$$

where f_1, f_1', f_1'', and f_1''' are the values of the function to be interpolated at the first point node and its first, second, and third derivatives, respectively, and h is the distance between points. It shall be noted that the order of accuracy used could be selected to be higher. Using Taylor series expansions, it is possible to find the derivatives at the first node by using a backward difference formula and the derivatives at the last node, N, by using a forward difference formula. Then, Eq. (14) result in a system of four linear equations from which it is possible to obtain the values of f_1, f_2, f_{N-1}, and f_N that improve the periodicity of the data set to be interpolated.

3.3 Constraint formulation

The solution of the optimization algorithm must fulfill a set of constraints as stated at the beginning of this Chapter. The set of constraints is summarized as follows.

1. Neural excitations must be bounded in the interval [0, 1]. This kind of constraint ensures that muscle forces are consistent with the activation and contraction dynamics of the muscles.
2. Ground clearance must be positive or equal to zero to ensure no penetration of the feet into the ground.
3. Positive normal contact forces to avoid bilateral constraints between the feet and the ground.
4. Tangent contact forces on the feet must be consistent with Coulomb's friction model to avoid foot sliding.
5. The averaged velocity is fixed.
6. Design variables are bounded. These bounds may be due to some physiological reasons like for example the amplitud of the relative motion allowed by a certain joint.
7. Other physiological constraints that may help to the convergence of the optimization algorithm like for instance constraining the maximal achieved knee flexion during the swing phase or the maximal achieved hip extension during the stance phase, see Ackermann [1].
8. Equations of motion must be fulfilled according to a certain tolerance.
9. Kinematic constraints must be fulfilled within a certain tolerance.

Exactly satisfying the equations of motion, although it would be desirable, seems to be extremely difficult. One reason for that is the parameterization of the motion and muscle forces by using splines. Doing so, we are assuming a certain error in the representation of the motion since it does not have to be a combination of splines polynomials. Therefore, we have to accept a small violation of the equations of motion. In order to quantify such an infringement, the constraints are formulated in terms of joint torques since we know approximately the usual range of values from inverse dynamics of normal walking. In what follows, the optimization constraints of the equations of motion are formulated.

As it has been stated, muscle forces as well as generalized coordinates are considered as design variables. This means that during the iterative solution of the optimization problem, we will have generalized coordinates and muscle forces that are not completely consistent. In case we have a consistent set of muscle forces and generalized coordinates, the following system of equation holds

$$\boldsymbol{M}\ddot{\boldsymbol{q}} + \boldsymbol{k} = \boldsymbol{q}_r + \boldsymbol{B}\boldsymbol{A}\boldsymbol{f}^m + \boldsymbol{C}_{ph}^T \boldsymbol{\lambda}_{ph} \tag{15}$$

Then, we know that there is a unique set of Lagrange multipliers $\boldsymbol{\lambda}_{ph}$ for each phase of the motion that can be calculated for example by using the pseudo-inverse of the Jacobian matrix of the constraints, see Strang [23], as

$$\boldsymbol{\lambda}_{ph} = \left(\boldsymbol{C}_{ph}^T\right)^+ \left(\boldsymbol{M}\ddot{\boldsymbol{q}} + \boldsymbol{k} - \boldsymbol{q}_r - \boldsymbol{B}\boldsymbol{A}\boldsymbol{f}^m\right) \tag{16}$$

In case the motion and the muscle forces are not fully consistent, the previous equation provides an estimation of the Lagrange multipliers in a least square sense [23] and for that reason it is denoted as

$$\boldsymbol{\lambda}_{ph}^* = \left(\boldsymbol{C}_{ph}^T\right)^+ \left(\boldsymbol{M}\ddot{\boldsymbol{q}} + \boldsymbol{k} - \boldsymbol{q}_r - \boldsymbol{B}\boldsymbol{A}\boldsymbol{f}^m\right) \tag{17}$$

Due to this inconsistence between the motion and the muscle forces, we have to accept a certain error $\boldsymbol{e}_m$ in the equations of motion

$$\boldsymbol{M}\ddot{\boldsymbol{q}} + \boldsymbol{k} = \boldsymbol{q}_r + \boldsymbol{B}\boldsymbol{A}\boldsymbol{f}^m + \boldsymbol{C}_{ph}^T \boldsymbol{\lambda}_{ph}^* + \boldsymbol{e}_m \tag{18}$$

Then, using Eqs. (17, 18), and the pseudo-inverse of $\boldsymbol{C}_{ph}^T$, one can write

$$\boldsymbol{C}_{ph}^T \boldsymbol{\lambda}_{ph}^* = \boldsymbol{C}_{ph}^T \boldsymbol{\lambda}_{ph}^* + \boldsymbol{e}_m \rightarrow \left(\boldsymbol{C}_{ph}^T\right)^+ \boldsymbol{e}_m = \boldsymbol{0} \tag{19}$$

It shall be noted here that the number of components of vector $\boldsymbol{e}_m$ is equal to the number of generalized coordinates while the number of rows of matrix $\left(\boldsymbol{C}_{ph}^T\right)^+$ is the number of active constraints, n_a, at the phase ph of motion. In the previous equation, it has been used that $\left(\boldsymbol{C}_{ph}^T\right)^+ \boldsymbol{C}_{ph}^T = \boldsymbol{I}$ since, due to the non-redundant set of kinematic constraints used, the columns of $\boldsymbol{C}_{ph}^T$ are independent.

As it was said at the beginning of this section, the constraints coming from the equations of motion are formulated in terms of joint torques. Thus, the torques at the joints can be evaluated from the muscle forces as

$$\boldsymbol{\tau}^m = \boldsymbol{A}\boldsymbol{f}^m \tag{20}$$

where $\boldsymbol{\tau}^m$ is the vector of joint torques with a number of components, n_b, equal to the number of actuated joint angles. On another hand, the torques can be calculated by using the estimated Lagrange multipliers of Eq. (17) as

$$\boldsymbol{\tau}^* = \boldsymbol{B}^+ \left(\boldsymbol{M}\ddot{\boldsymbol{q}} + \boldsymbol{k} - \boldsymbol{q}_r - \boldsymbol{C}_{ph}^T \boldsymbol{\lambda}_{ph}^* \right) \tag{21}$$

Now, substituting Eqs. (18) into (21) and using the properties of the pseudo-inverse once more, one has

$$\boldsymbol{\tau}^* = \boldsymbol{B}^+ \left(\boldsymbol{B}\boldsymbol{\tau}^m + \boldsymbol{e}_m \right) \tag{22}$$

what, in case that $\boldsymbol{B}$ has independent columns and there is a full consistence between muscle forces and motion ($\boldsymbol{\tau}^m = \boldsymbol{\tau}^*$), leads to

$$\boldsymbol{B}^+ \boldsymbol{e}_m = \boldsymbol{0} \tag{23}$$

It is worth of noting here that the number of linear equations in (23) is equal to the number of actuated joints n_b.

Equations (19) and (23) form a system of $n_a + n_b$ linear equations. It can be concluded that $\boldsymbol{e}_m = \boldsymbol{0}$ if $n_a + n_b$ is larger than the number of generalized coordinates, and therefore, if $\boldsymbol{\tau}^m = \boldsymbol{\tau}^*$, then $\boldsymbol{e}_m = \boldsymbol{0}$. However, $n_a + n_b$ is not always larger than the number of generalized coordinates in all phases of motion. For example, in the work of Ackermann [1], the planar model studied has $n_a = 2$ kinematic constraint equations in phases 4 and 8. Since the number of actuated joints is $n_b = 6$ and the number of generalized coordinates is 9, it is not possible to fulfill all the constraints of motion by having $\boldsymbol{\tau}^m = \boldsymbol{\tau}^*$. The three-dimensional model used in this research work has $n_a = 5$ in phases 3 and 7 and $n_a = 4$ in phases 4 and 8 and again the equality $\boldsymbol{\tau}^m = \boldsymbol{\tau}^*$ does not guaranty that $\boldsymbol{e}_m = \boldsymbol{0}$. Therefore, the constraint $\left| \boldsymbol{\tau}_i^m - \boldsymbol{\tau}_i^* \right| \leq \varepsilon_m$, being ε_m a certain tolerance, cannot be used to ensure $\boldsymbol{e}_m$ to be small enough throughout the whole walking cycle.

In order to ensure the fulfillment of the equations of motion, the error is defined using the generalized force vector associated with joint torques instead of the vector of torques itself. This can be done since the terms of the generalized force vector of the joint torques acting on the coordinates describing the absolute motion of the trunk and pelvis with respect to the inertial frame are zero. This way, the generalized force vector of the joint torques can be obtained from muscle forces

$$\boldsymbol{q}^m = \boldsymbol{B}\boldsymbol{A}\boldsymbol{f}^m, \tag{24}$$

and from the estimated Lagrange multipliers according to (15) or (18), respectively

$$\boldsymbol{q}^* = \boldsymbol{M}\ddot{\boldsymbol{q}} + \boldsymbol{k} - \boldsymbol{q}_r - \boldsymbol{C}_{ph}^T \boldsymbol{\lambda}_{ph}^*. \tag{25}$$

The optimization constraint of the equations of motion is now written as

$$\left| \boldsymbol{q}_i^m - \boldsymbol{q}_i^* \right| \leq \varepsilon_m \quad i = 1,\ 2, \ldots, n_c, \tag{26}$$

where ε_m is the tolerance of the constraint satisfaction. The error term to be bound at each control point is

$$e_{i,j}\left(\boldsymbol{\chi}\right) = \left(\boldsymbol{q}_i^m - \boldsymbol{q}_i^* \right)_j \tag{27}$$

what, according to Eq. (26), leads to two constraints per control point and per each component of the generalized joint torque vector as follows

$$\begin{aligned} e_{i,j}\left(\boldsymbol{\chi}\right)/\varepsilon_m - 1 &\leq 0 \\ -1 - e_{i,j}\left(\boldsymbol{\chi}\right)/\varepsilon_m &\leq 0 \end{aligned} \tag{28}$$

Of course, this formulation results into a larger number of constraints of the equations of motion per control point as compared to the formulation used by Ackermann [1], who defined the violation of the constraint by taking the maximum of the norm of the error at control points as

$$\max\left(\left| \boldsymbol{e}_j\left(\boldsymbol{\chi}\right) \right| \right) \leq \varepsilon_m \qquad j = 1,\ 2, \ldots, n_b \tag{29}$$

Even if the number of constraint equations is increased, the formulation used in this research leads to a better possed constrained optimization problem. Using Eq. (28), the constraints of the equations of motion are continuous and the Jacobian of the constraints provides a better information when searching for the optimum, what results in a smaller number of iterations of the optimization algorithm.

4 Numerical results

This Chapter shows some numerical results of the simulations carried out using the optimization framework presented. First, a two-dimensional symmetrical model has been analyzed to check the performance of the approach and the convergency of the model for different parameterizations. Later, non-symmetrical models are analyzed. The first is two-dimensional non-symmetrical while the second is three-dimensional, both of them including unilateral disorders.

4.1 Two-dimensional symmetrical model

A two-dimensional symmetrical (2DS) model can also be found in the work of Ackermann [1], and therefore, a comparison of the numerical results and performance is possible. Since many improvements are introduced, the comparison serves also to validate the added modifications.

The two-dimensional model used in this section is modeled by using 9 coordinates and 7 bodies. A sketch of the model can be seen in Fig. 4. As it is shown, the model is contained in the sagittal plane. The symmetry of the model allows a big simplification in the number of optimization variables. In fact, it is assumed that the left leg experiences in the second half of the walking cycle the same motion as the right leg in the first half. In addition, the motion of the pelvis is assumed to be the same in both halves of the cycle. Muscle forces of the left leg are exactly the same as those of the right one but shifted half a walking cycle. Therefore, the symmetrical model is represented by the generalized coordinates of the pelvis during the first half of the walking cycle and the generalized coordinates and muscle forces of the right leg during the whole walking cycle.

Table 2 shows the results of several models that differ one to another in the number of nodes used to parameterize the generalized coordinates and muscle forces. Every model has an odd number of nodes in order to have a node exactly at the time instant equal to half of the walking period. Thus, the number of nodes ranges from 19 to 35. The convergency of the different models to a unique solution is remarkable. As can be observed in Table 2, increasing the number of nodes always leads to a smaller difference in the value of the cost function f. The same behavior is observed in the values of the metabolical cost of transportation, E^t, and the deviation from normal walking pattern, J_d measured in the lab.

The last column of data in Table 2 shows the computation time required for each model. In the case of the 27 and 35 nodes models, the computation times could not be feasibly measured due to other processes running

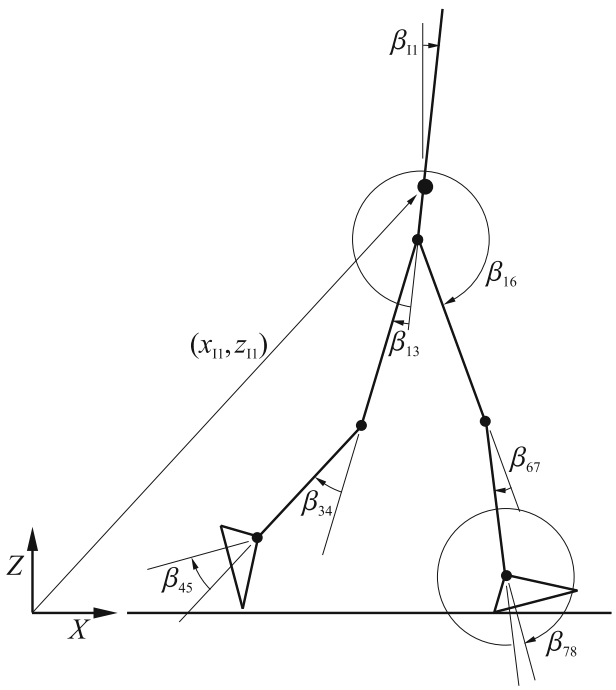

Fig. 4 Sketch of the two-dimensional model with its generalized coordinates

Table 2 Performance of the different models

NN	f	E^t (J/m)	J_d	CT (h)
19	13.33	626.00	7.07	0.55
21	7.54	415.73	3.38	1.85
23	6.52	351.01	3.01	2.87
25	5.50	310.62	2.39	3.25
27	4.99	283.28	2.16	5.65[a]
29	4.62	254.22	2.08	8.66
31	4.45	246.32	1.99	9.52
33	4.37	238.57	1.98	13.17
35	4.31	236.10	1.95	16.16[a]

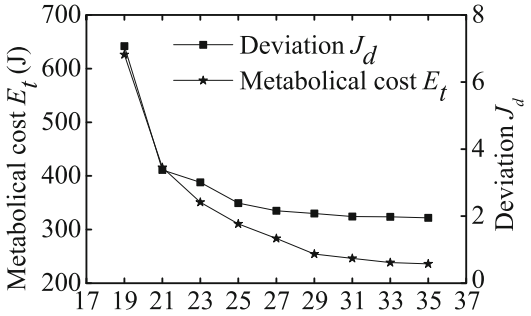

NN stands for number of nodes, f is the cost function, E^t is the metabolical cost of transportation, J_d is the measure of deviation from normal walking patterns, CT stands for computation time

[a] Estimated CT values

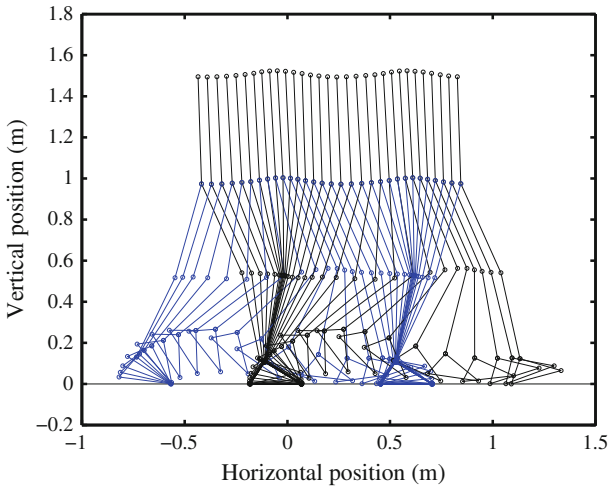

Fig. 5 Different positions of the 2D walker during a gait cycle. The *left* leg is identified by positions −0.5 and 0.5 m, the *right* leg is found at positions −0.1 and 1.0 m

on the same computer, and their values have been estimated by fitting a polynomial to the rest of values. The tolerances for the fulfillment of the equations of motion and of the kinematical constraints were $\varepsilon_m = 2$ Nm and $\varepsilon_k = 2$ mm as in the work of Ackermann [1]. On another hand, the termination tolerances for the SQP optimization algorithm were fixed to $TolFun = 10^{-4}$, $TolCon = 10^{-4}$, and $TolX = 10^{-6}$, being $TolFun$ the termination tolerance for the cost function, $TolCon$ the termination tolerance for the constraints violation, and $TolX$ the termination tolerance for design variables vector. The computation times shown in Table 2 have been obtained using a processor Intel® Xeon® CPU E5530 at 2.40 GHz with 4 cores and 6 GiB RAM. It has been observed that the pre-computation of the matrices involved in the spline interpolation, the elimination of numerical differentiation, and the proper formulation of the equations of motion and kinematical constraints have helped to reduce the computation time to achieve a converged solution. Figure 5 shows different positions of a walker during a gait cycle simulated using 29 nodes.

It is worth of mention that the values of the metabolical cost of transportation, E^t, and the deviation from the normal measured motion, J_d, do not coincide with the values reported by Ackermann [1]. These differences can be due to the different parameterization used in this research and the different definition of the measure of the deviation from normal walking. Ackermann [1] used the standard deviation to scale the deviation from simulated values and measured ones, while the mean square deviation from the mean value has been used in this research. The weighting factors w_E and w_J used here are both equal to 1. As shown by Ackermann [1], a difference in the mentioned weighting factors may lead to different values of the optimized magnitudes, i.e., the metabolical cost of transportation, E^t, and the deviation from measured motion, J_d.

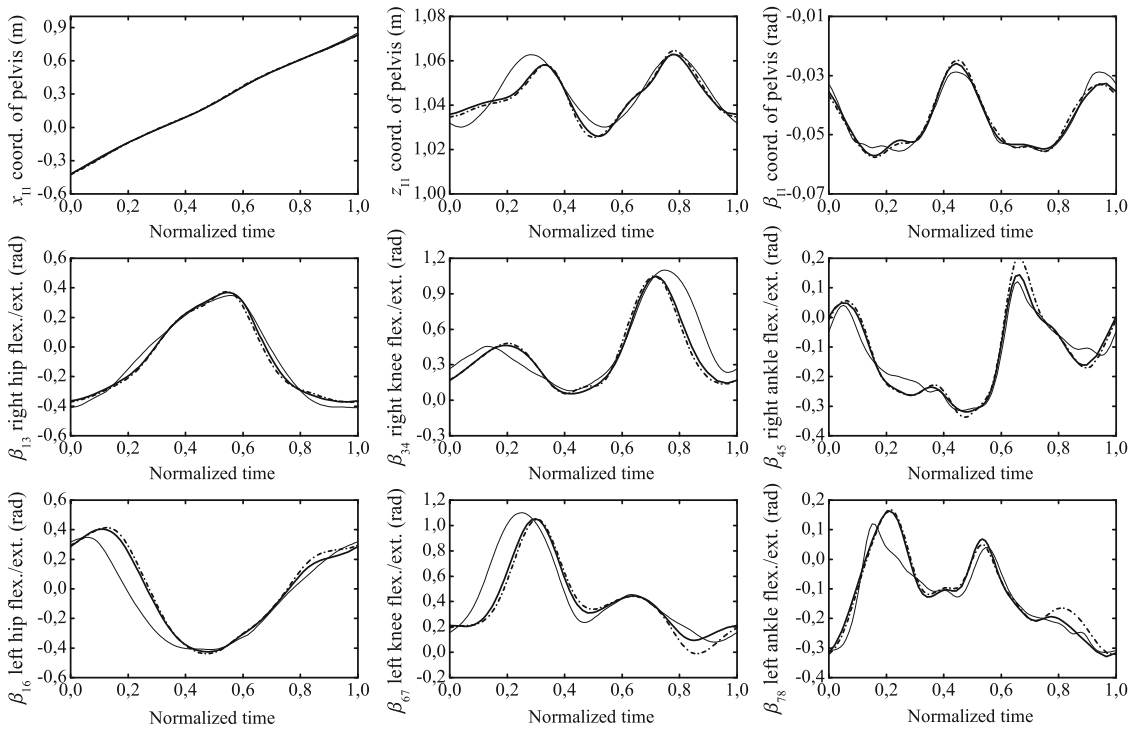

Fig. 6 Time histories of the generalized coordinates of the 35 nodes symmetrical model solution (*solid thin line*), of the 18 nodes 2DNS model (*solid thick line*) and of the 18 nodes 2DNS model with one-sided disorder (*dash dot thick line*)

4.2 Two-dimensional non-symmetrical model

A two-dimensional non-symmetrical (2DNS) model as the one represented in Fig. 4 is tested in this section against one-sided disorders. In this case, the disorder consists of an increase in the weight of the right foot by 2 kg. In principle, one-sided disorders are expected to cause walking motions that cannot be described in the sagittal plane anymore even though the human being tries to keep as vertical as possible for stability reasons and to walk as normal as possible for esthetic reasons. The behavior of the 2DNS model in presence of a one-sided disorder is studied here and later compared with that of a three-dimensional model. The main advantage of the 2DNS model is it ability to reproduce non-symmetrical motions while keeping a reasonable computational complexity.

As was mentioned before, the measured walking motion is not perfectly symmetrical. In order to study the influence of one-sided disorders, a fully symmetrical walking motion is taken from a 35 nodes symmetrical model and used as reference motion. The symmetrical motion used is kinematically and dynamically consistent with the musculoskeletal model used in this section. Therefore, a loss of symmetry cannot be induced by the reference motion. Figure 6 shows the time histories of the generalized coordinates describing the two-dimensional motion for the reference solution (solid thin line), a 18 nodes solution of the 2DNS model with symmetrical inertial properties (solid thick line) and a 18 nodes solution of the 2DNS model with unsymmetrical inertial properties due to an artificial weight of 2 kg attached to the right foot (dash dot thick line). It can be seen that both models (with and without the 2 kilos weight) follow the reference motion. However, the disordered motion shows some differences around the 50% of the cycle when the right foot must be elevated. Since its weight increases the natural trend to decrease its elevation and therefore, increase the right ankle rotation at phases 4, 5, and 6. As a consequence, the left leg has to adapt to this situation by extending the knee and increasing the left ankle flexion at the left leg stance phase.

Interestingly, the model used is able to describe the adaptation motion of both legs. As it is expected, the disordered model shows a higher metabolical cost of transportation (418.49 J/m) and also a higher deviation (3.07) from the reference motion than the model with symmetrical inertial properties (374.94 J/m and 2.11, respectively).

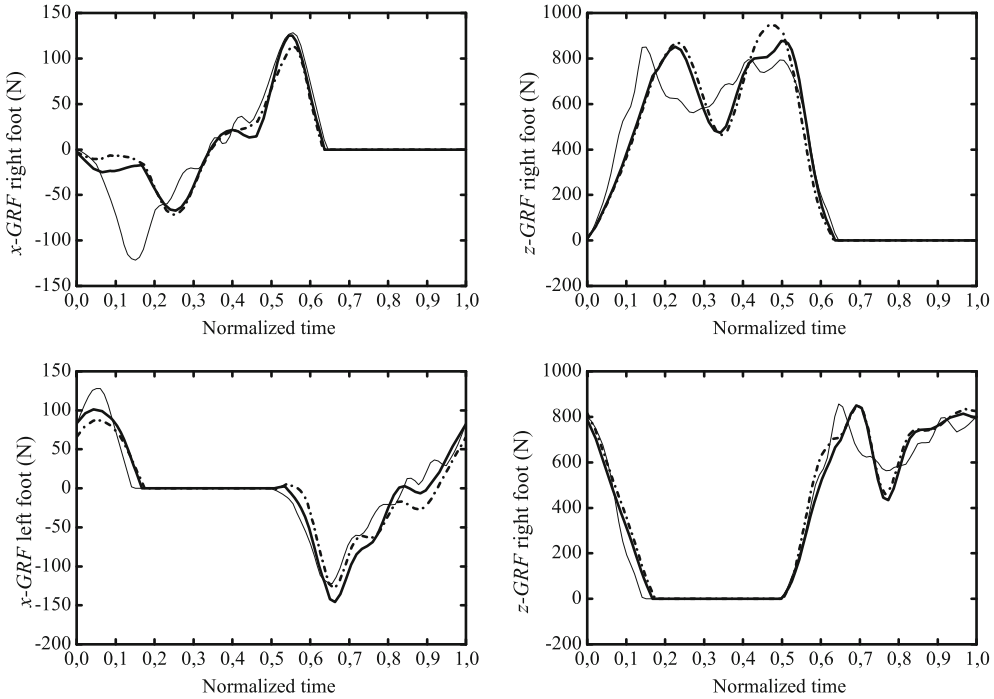

Fig. 7 Time histories of the ground reaction forces of the 35 nodes symmetrical model solution (*solid thin line*), of the 18 nodes 2DNS model (*solid thick line*) and of the 18 nodes 2DNS model with one-sided disorder (*dash dot thick line*)

Figure 7 shows the time histories of the normal and tangent contact forces at the feet for the reference solution, the symmetrical and the disordered walking motions. The most significant feature is the increase in the right foot normal force at the end of the right leg stance phase due to the attached weight. The contact forces at the left foot are quite similar to those of the model with symmetric inertial properties.

Figure 8 shows a comparison of the neural excitations corresponding to the muscles of the right leg with (dash dot line) and without (solid line) the attached weight. It can be seen that the main effect of increasing the weight of the foot is a wider and higher activation of some of the right leg muscles, what results in a larger metabolical energy cost. The simulated motions allow a certain level of co-contraction, for example, at the first 20% of the cycle for the *tibialis anterior* (TA), *soleus* (SOL), and *gastrocnemius* (GAS). However, the peak of the TA muscle coincides with a zero value of its antagonists with respect to the ankle joint, muscles GAS and SOL, what seems to be energetically efficient since the coincidence of two peaks of antagonist muscles would result in a silly waste of energy. In the case of the weighted motion, a similar situation happens for the RF and HAM, which are antagonist with respect to the hip joint, at the final 40% percent of the cycle.

The 2DNS model has a very limited applicability since it is reduced to motions that can be described in the sagittal plane. Of course, unilateral disorders are mainly affecting the balance in the frontal plane and, for this reason, a three-dimensional non-symmetrical model is a more appropriate choice. However, it is interesting to study how much information can be extracted from the much less expensive 2DNS model.

4.3 Three-dimensional non-symmetrical model

In the three-dimensional non-symmetrical (3DNS) model studied in this section, see Fig. 1, all generalized coordinates and muscle forces are considered independent. This fact significantly increases the size of the model, and in order to keep the computation time as small as possible, only 18 nodes are used to parameterize each time-dependent variable. However, the optimization algorithm used took up to 65 h to find a solution within tolerances of $TolX = 10^{-4}$, $TolFun = 10^{-2}$, and $TolCon = 10^{-2}$, what requires the scaling of constraints and design variables to ensure the enough accuracy of the constraint satisfaction. In this case, the measured motion has been used as a reference motion or normal walking pattern, respectively. Two similar 18 nodes 3DNS models are solved with one of them having a weight of 2 kg attached

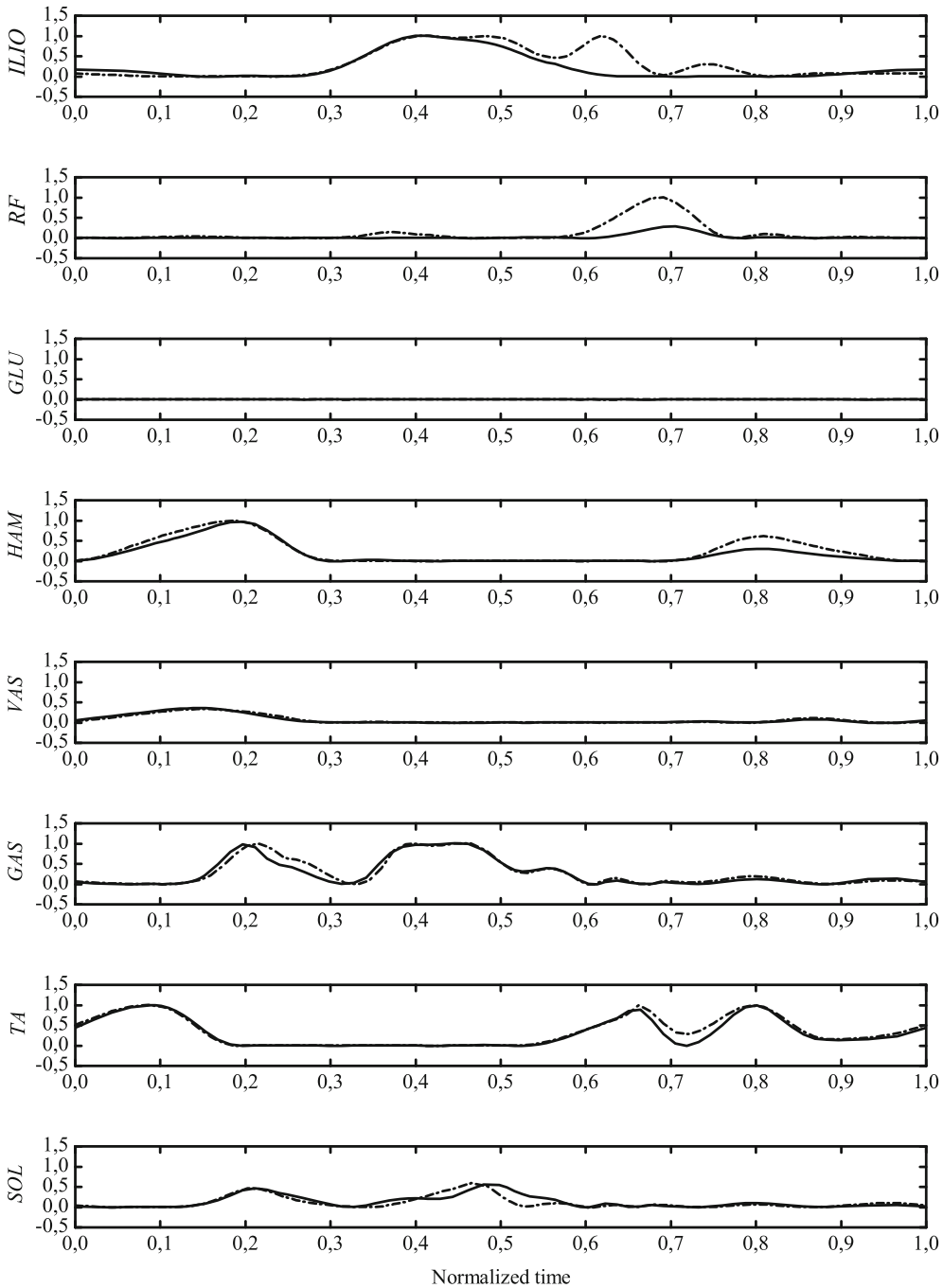

Fig. 8 Neural excitation time histories of normal (*solid line*) and disordered (*dash dot line*) walking motions

to the right foot. The simulations results are shown in Figs. 9, 10, 11, 12, and 13 together with experimentally measured results. As shown by the two-dimensional model the attachment of a weight to the ankle results in a higher energy expenditure during walking. The metabolical cost of transportation of the model without the attached weight is 569.56 J/m while 631.14 J/m are obtained when the weight is attached. On another hand, the deviation from normal walking patterns increased from 3.06 to 3.40 when the weight is attached.

In detail, the time histories of the generalized coordinates of the two models are shown in Figs. 9 and 10 together with the experimentally measured motion. As in the symmetrical model, the motion in the sagittal

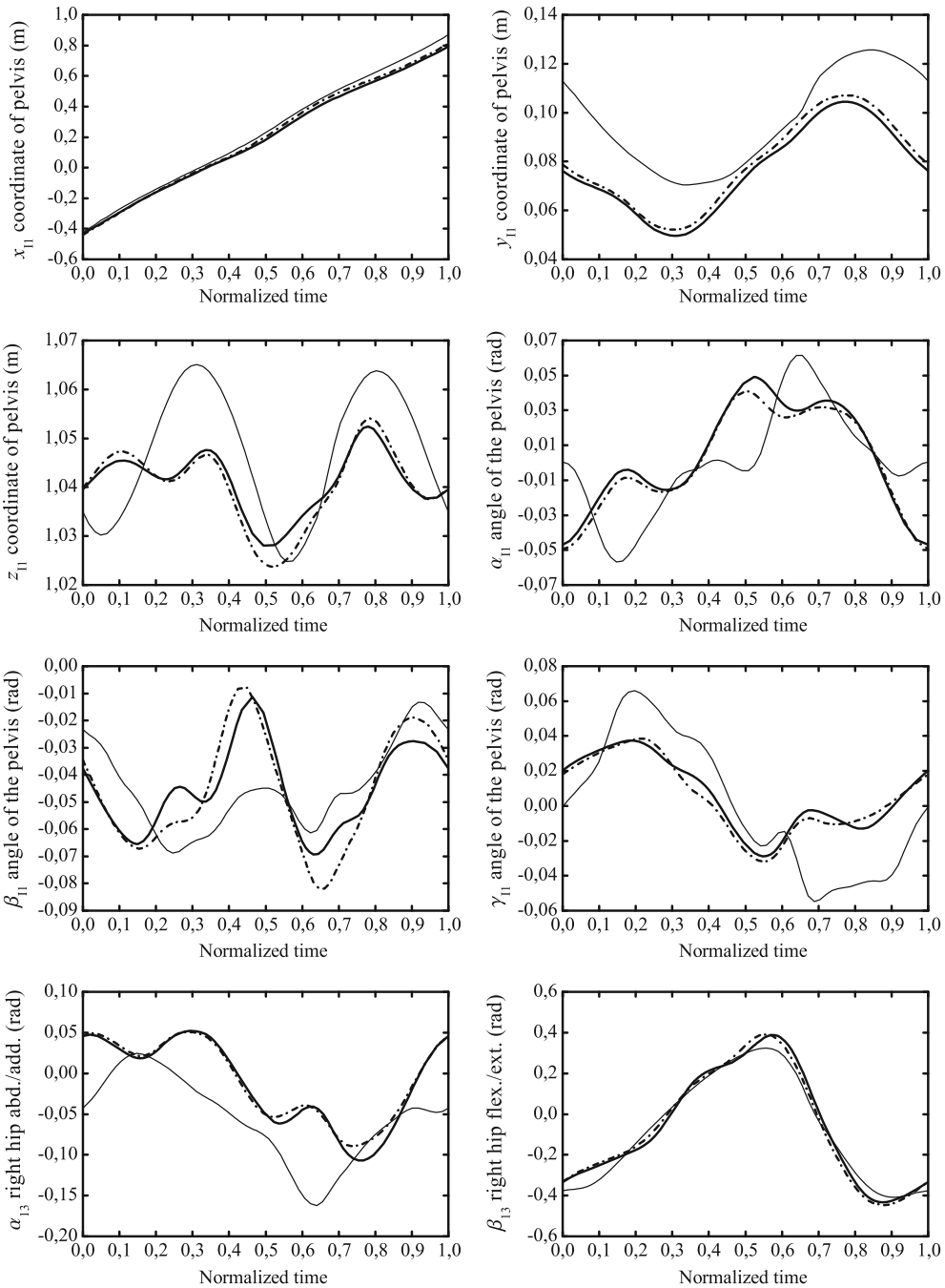

Fig. 9 Time histories of the generalized coordinates experimentally measured (*solid thin line*), simulated with the 18 nodes 3DNS model (*solid thick line*) and with the 18 nodes 3DNS model with one-sided disorder (*dash dot thick line*)

plane is approximately captured by the 3DNS model while there are some differences in the motion out of the sagittal plane. The influence of the attached weight can be noticed in the pitch rotation of the pelvis-trunk (HAT) body, β_{I1}, in the second half of the cycle.

Again, due to the increased weight of the right foot, the natural trend is to decrease the right foot elevation in the second half of the cycle. As it was pointed out in the 2DNS model, the maximum rotation (dorsiflexion) increases as it is shown in Fig. 10. The effect of this alteration in the gait pattern on the left leg is slightly different than in the 2DNS model. In this case, there is an increase in the left knee and left ankle flexion but it is less significant than in the 2DNS model because the 3DNS model can now slightly modify also the

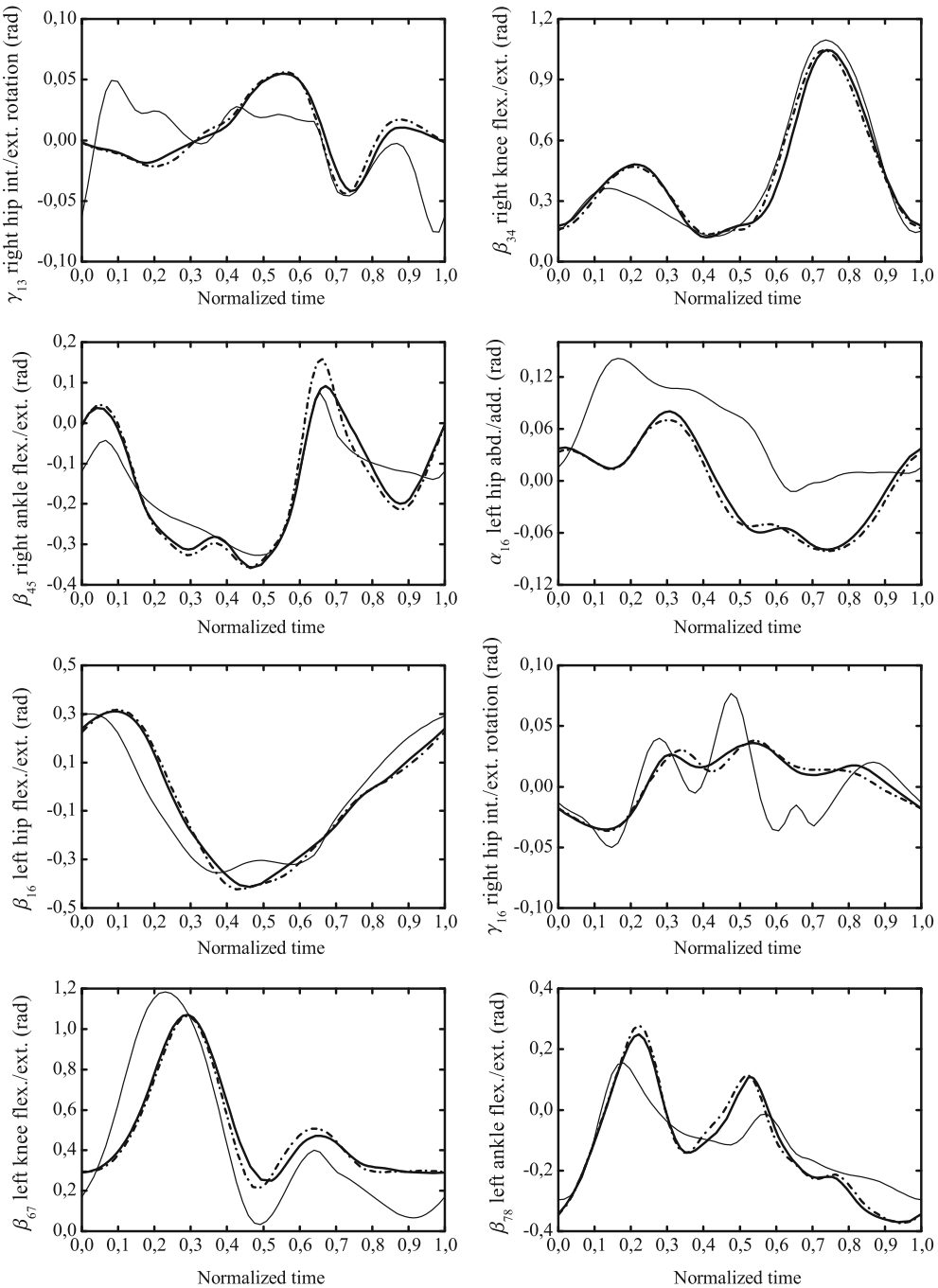

Fig. 10 Time histories of the generalized coordinates experimentally measured (*solid thin line*), simulated with the 18 nodes 3DNS model (*solid thick line*) and with the 18 nodes 3DNS model with one-sided disorder (*dash dot thick line*)

three rotations at the hip. Therefore, the 3DNS model can absorb the effect of the disorder introduced without significantly modify the motion of the left leg.

Figure 11 shows the time histories of the three components of the ground reaction forces at both feet. The similarity between the solutions with and without the attached weight is remarkable. The solutions are now coinciding better than in the 2DNS model, because of the aforementioned ability of the 3DNS model to accept minor variations of its variables to absorb the effect of one-sided disorders. Enforcing the model to follow a certain symmetrical motion makes the simulated motion to maintain the same level for the normal contact

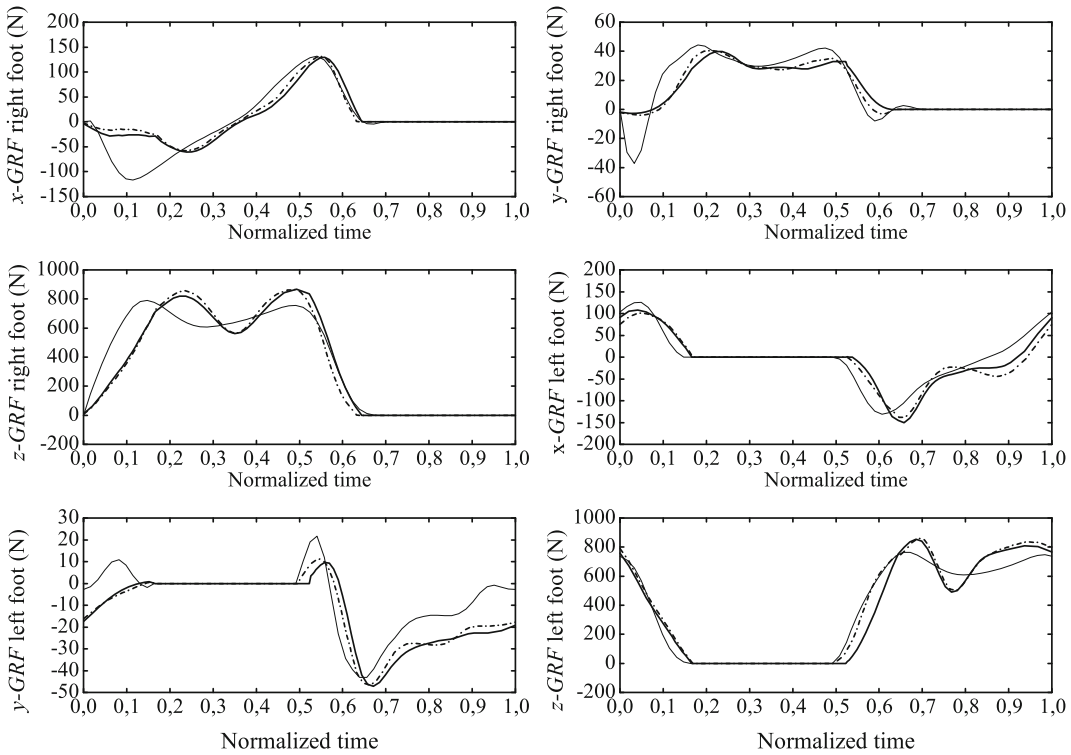

Fig. 11 Time histories of the ground reaction forces experimentally measured (*solid thin line*), simulated with the 18 nodes 3DNS model (*solid thick line*) and with the 18 nodes 3DNS model with one-sided disorder (*dash dot thick line*)

force by adapting the time histories of the generalized coordinates accordingly. Changing the weight factors in Eq. (13) to give less importance to the motion to be followed, this effect could be reduced.

The different neural activation time histories of the muscles of the right and left legs of the 18 nodes 3DNS model are shown in Figs. 12 and 13, respectively. It can be observed a higher neural excitation level of the TA muscle between 60 and 70% of the cycle coinciding with the increase in the maximum dorsiflexion at the right ankle. Also, the adaptation of the left leg requires higher activation levels of the left leg muscles, but the changes are less visible than in the 2DNS mode.

As shown in this section, the 3DNS model provides much richer information of the dynamics of human gait with one-sided disorders. The model could also be improved by adding extra degrees of freedom to better represent the upper limb motion offering new research directions.

5 Conclusions

Based on the research carried out and on the numerical results obtained, the following conclusions could be drawn.

Formulating the equations of motion of the musculoskeletal system by using NewEul-M^2 is very important since it was possible to obtain the equations of the system symbolically with a minimum number of generalized coordinates and joint constraints. However, the symbolical manipulation of the equations was a limiting factor for the complexity of the model finally used.

It was possible to decrease the computational effort of the spline interpolation problem by reducing the size of the problem after some algebraic manipulations and by pre-computing the most expensive part of the information required (the most expensive part) to evaluate the interpolated function before the optimization algorithm starts.

The errors coming from numerical differentiation and the non-uniform distribution of such errors are avoided by analytical differentiation. The numerical differentiation via finite difference formulae is eliminated by implementing the first and second time derivatives of the interpolating polynomials and by obtaining the analytical derivatives of the contractile element force law.

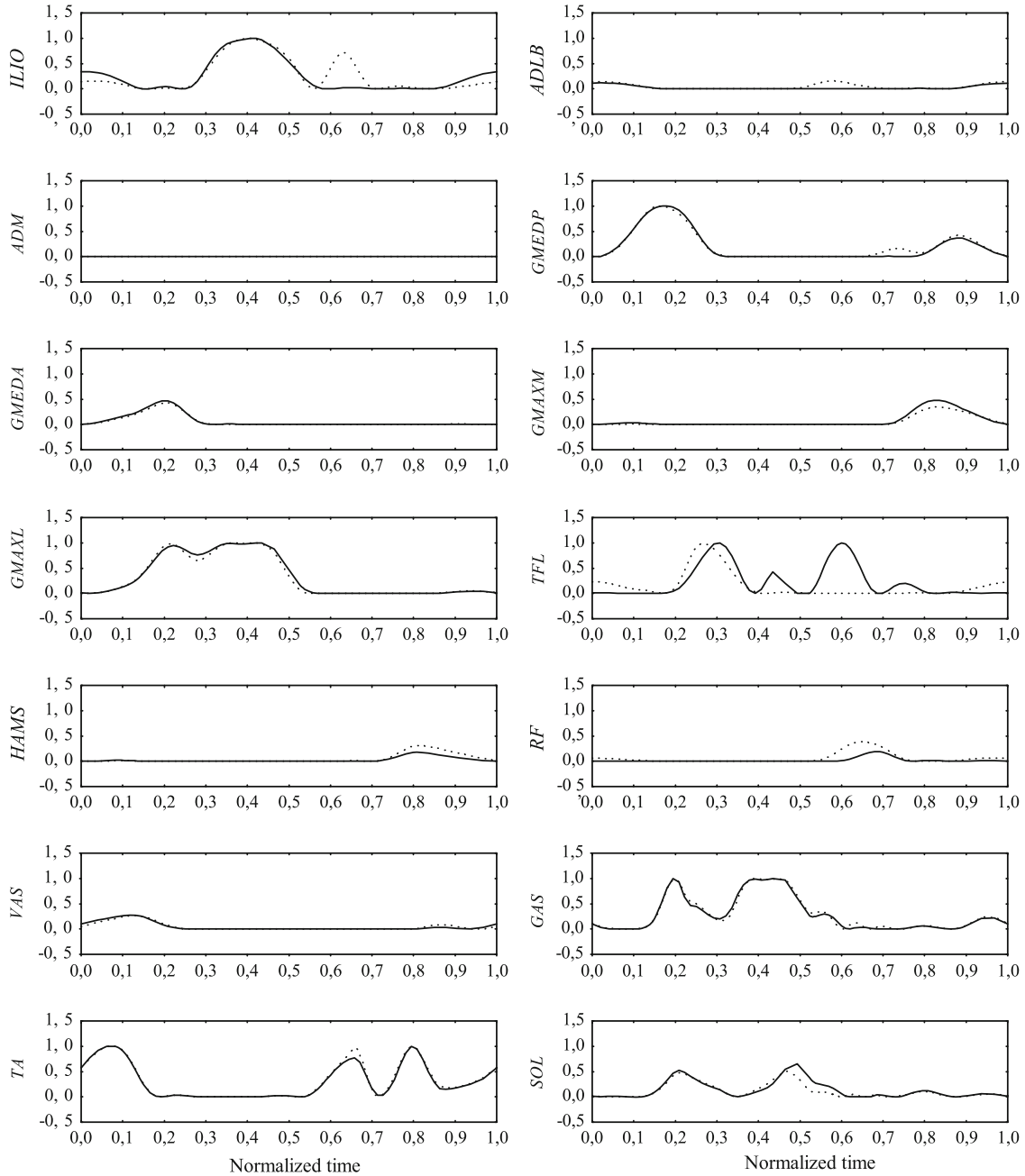

Fig. 12 Neural excitations of the *right* leg muscles with (*dotted line*) and without (*solid line*) wearing the 2 kg weight

The number of muscles is reduced by grouping muscles with the same mechanical function in muscles groups. This allows a reduction in the number of design variables of the optimization problem without decreasing the possibilities of motion of the model.

The number of iterations of the optimization algorithm is reduced by formulating the constraints associated with the equations of motion and with the kinematic constraints at all control points. Even if the number of constraints of the constrained optimization problem is increasing, the saving in time due to the decrease in the number of iterations justified the implementation of such constraints.

Formulating the constraints of the phases of the motion in which the musculoskeletal system is underactuated by using no external torques at the metatarsophalangeal joint leads to a solution very similar to the one obtained by adding such torques. Using no external torques is more consistent with the approach used,

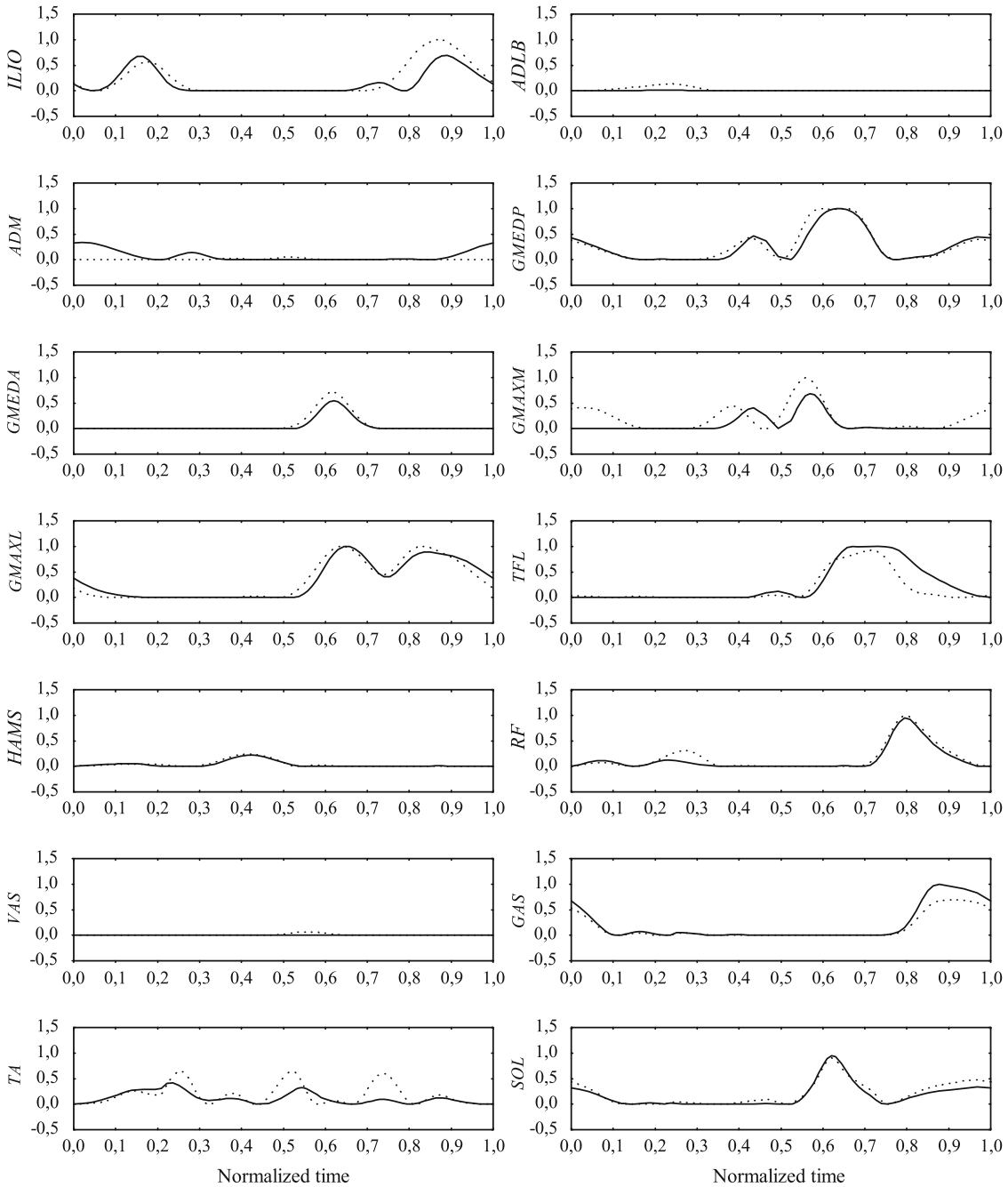

Fig. 13 Neural excitations of the *left* leg muscles with (*dotted line*) and without (*solid line*) wearing the 2 kg weight

in which each muscle must behaves according to its own activation and contraction dynamics and contributes to the total metabolical cost of transportation.

The two-dimensional non-symmetrical model of the musculoskeletal system may be used to analyse the influence of non-severe one-sided disorders as long as the motion of the human body remains in the sagittal plane. The natural trend to keep the walking pattern as close as possible to healthy patterns allows that the two-dimensional non-symmetrical model may still be used in such situations. However, more severe disorders can only be studied with three-dimensional models.

The three-dimensional symmetrical model showed the importance of modeling the trunk and pelvis as different bodies. Not doing so results in a very reduced motion of the pelvis-trunk body since the natural

compensation of the pelvis rotation by counter rotation of the trunk cannot be represented. The three-dimensional symmetrical model with a single pelvis-trunk body shows a very small motion out of sagittal plane.

The three-dimensional non-symmetrical model showed a better adaptation to one-sided disorders than the two-dimensional non-symmetrical model. In the three-dimensional non-symmetrical model, the presence of an attached mass at one foot is compensated by smaller variations of more generalized coordinates. As a result, the differences in the simulated ground reaction forces of two three-dimensional non-symmetrical models with and without an attached weight are smaller than in the two-dimensional two-symmetrical model. This fact shows the importance of including three-dimensional dynamical effects when simulating one-sided disordered walking patterns.

Including the metabolical energy expenditure and the activation and contraction dynamics of muscles in the simulation method allows the possibility to study coordination aspects of human walking and shows a potential application of this approach to the design of rehabilitation therapies and to the design of assistive devices. Efficient methods as presented in this research for the simulation of human walking are most important for the development of rehabilitation therapies and the design of assistive devices.

Acknowledgments This research was supported in part by the Spanish Ministry of Science and Innovation through the grant 2008-0249 and through the project DPI2009-11792. This support is gratefully acknowledged.

Conflict of interest The authors do not have any conflicts of interest with regard to this paper and the materials contained herein.

Appendix A: Muscles spanning the musculoskeletal model

This appendix shows the data used to model the different muscles of the musculoskeletal model. All these parameters are estimated from Refs. [1,6,15] for a subject with a height of 1.80 m and a weight of 75 kg.
In Table 3 SOL stands for *Soleus*, TA for *Tibialis anterior*, GAS for *Gastrocnemius*, VAS for *Vastii*, RF for *Rectus femoris*, HAMS for *Hamstrings*, TFL for *Tensor fascia latae*, GMAXL for *Gluteus maximus lateral*, GMAXM for *Gluteus maximus medial*, GMEDA for *Gluteus medius anterior*, GMEDP for *Gluteus medius posterior*, ADM for *Adductor magnus*, ADLB for *Adductor longus brevis* and ILPSO for *Ilipsoas*. From the data in Table 3, the length of the different muscles is calculated as follows:

$$l_r = l_0 - r_{h\alpha}\alpha_{13} - r_{h\beta}\beta_{13} - r_{h\gamma}\gamma_{13} - r_{k\beta}\beta_{34} - r_{a\beta}\beta_{45} \tag{A.1}$$

$$l_l = l_0 + r_{h\alpha}\alpha_{16} - r_{h\beta}\beta_{16} + r_{h\gamma}\gamma_{16} - r_{k\beta}\beta_{67} - r_{a\beta}\beta_{78} \tag{A.2}$$

where l_r and l_l are the lengths of muscles of the right and left legs, respectively.

Table 3 Muscle group properties, being $f^m_{\max}$ the maximum muscle force

Muscle group	$f^m_{\max}$ (N)	l^{ce}_{opt} (m)	l_{slack} (m)	α_p [°]	$r_{h\beta}$ (cm)	$r_{h\alpha}$ (cm)	$r_{h\gamma}$ (cm)	$r_{k\beta}$ (cm)	$r_{a\beta}$ (cm)	l_0 (cm)	ft (%)	width
SOL	3,883	0.055	0.254	23.6	0	0	0	0	5.30	28.4	20	1.039
TA	1,528	0.082	0.317	6	0	0	0	0	−3.70	40.6	25	0.442
GAS	1,639	0.055	0.420	14.3	0	0	0	2.00	5.30	48.7	45	0.888
VAS	7,403	0.093	0.223	4.4	0	0	0	−4.30	0	27.1	53	0.627
RF	1,320	0.114	0.320	5	−4.41	−1.14	−0.10	−3.82	0	41.2	55	1.443
HAMS	2,814	0.109	0.340	8	4.91	1.24	−0.33	4.17	0	44.3	45	1.197
TFL	262	0.095	0.425	3	−5.13	−3.82	2.67	0	0	53.1	30	0.560
GMAXL	1,730	0.145	0.106	2	3.32	−2.72	−1.96	0	0	20.6	55	0.625
GMAXM	686	0.154	0.120	5	5.13	2.25	−1.36	0	0	24.6	50	0.625
GMEDA	1,319	0.065	0.055	4	1.13	−1.94	4.11	0	0	10.6	50	0.625
GMEDP	1,215	0.065	0.048	7	2.06	−3.26	1.55	0	0	11.3	50	0.625
ADM	1,245	0.121	0.120	4	3.44	6.00	0.29	0	0	32.1	45	1.000
ADLB	994	0.128	0.042	6	−1.19	6.91	0.57	0	0	20.8	35	0.560
ILPSO	1,627	0.104	0.135	8	−3.31	−0.79	0.35	0	0	22.8	50	1.298

l^{ce}_{opt} the optimal length of the contractile element, l_{slack} the tendon length, α_p the pennation angle, $r_{h\alpha}, r_{h\beta}$ and $r_{h\gamma}$ the moment arms around the hip joint, $r_{k\beta}$ the moment arm around the knee joint, $r_{a\beta}$ the moment arm around the ankle joint, l_0 a parameter used to measure the muscle length, ft the percentage of fast twitch fibers and $width$ a parameter required to evaluate the contractile element force

Appendix B: Muscle contraction dynamics

The force-length-velocity relation used in this work is taken from the work of Nagano and Gerritsen [16], who adopted the formulae describing the muscle contraction dynamics from van Soest and Bobbert [26] and Cole et al. [10]. For the concentric contraction phase ($v^{ce} < 0$), the contractile element velocity v^{ce} is written as follows:

$$v^{ce} = -\Gamma\, l^{ce}_{opt} \left(\frac{(f_{isom} + A_{rel})\, B_{rel}}{\frac{f^{ce}}{a \cdot f^{m}_{max}} + A_{rel}} - B_{rel} \right) \tag{B.1}$$

where $\Gamma = \min(1, 3.33\, a)$. To simplify the inversion of the contraction dynamics, Ackermann [1] used a constant value for factor Γ equal to 1 obtaining consistent results. In this work, the same assumption for factor Γ is made. In Eq. (B.1), A_{rel} and B_{rel} are two muscle constant that may depend on the percentage of fast twitch fibers [25] or training conditions [16]. Typical values for this parameters used in [16] and [1] are $A_{rel} = 0.41$ and $B_{rel} = 5.2$. The force relative to f^{m}_{max} produced at isometric contraction, f_{isom}, is

$$f_{isom} = c \left(\frac{l^{ce}}{l^{ce}_{opt}} \right)^2 - 2c \left(\frac{l^{ce}}{l^{ce}_{opt}} \right) + c + 1 \tag{B.2}$$

being $c = -1/width^2$. Values for the $width$ parameter can be found in Nagano and Gerritsen [16]. On another hand, in the eccentric contraction phase ($v^{ce} > 0$), the contractile element velocity can be written as

$$v^{ce} = -l^{ce}_{opt} \left(\frac{c_1}{\frac{f^{ce}}{a \cdot f^{m}_{max}} + c_2} - c_3 \right) \tag{B.3}$$

being

$$\begin{aligned} c_1 &= \frac{\Gamma\, B_{rel}\, (f_{isom} + c_2)^2}{(f_{isom} + A_{rel})\, S_f} \\ c_2 &= -f_{isom}\, f_{asymp} \\ c_3 &= \frac{c_1}{f_{isom} + c_2} \end{aligned} \tag{B.4}$$

where f_{asymp} is the asymptotic maximum force value in the eccentric phase relative to f^{m}_{max} and S_f is the ratio between concentric and eccentric derivatives of force with respect to v^{ce}. In this work, $S_f = 1$ is used in order to enforce continuity of the slope of the force–velocity curve at $v^{ce} = 0$.

Appendix C: Muscle activation dynamics

The activation dynamics can be described according to Nagano and Gerritsen [16] by means of the first-order differential equation

$$\dot{a} = (u - a)\,(t_1 u - t_2) \tag{C.1}$$

where $t_2 = 1/t_d$ and $t_1 = 1/(t_a - t_2)$, being t_a and t_d the activation and deactivation time constants. Notice that if the activation and its time derivative are known, it is possible to calculate the neural excitation from Eq. (C.1) by solving a quadratic equation, which will be analyzed later.

References

1. Ackermann, M.: Dynamics and Energetics of Walking with Prostheses. PhD thesis, Institut für Technische und Numerische Mechanik, Stuttgart (2007)
2. Ackermann, M., Gros, H.: Measurements of Human Gaits. Technical Report of Zwischenbericht ZB-144, Institute of Engineering and Computational Mechanics, University of Stuttgart, 70550 Stuttgart (2005)
3. Ackermann, M., Schiehlen, W.: Dynamic analysis of human gait disorder and metabolical cost estimation. Arch. Appl. Mech. **75**(10–12), 569–594 (2006)
4. Al Nazer, R., Rantalainen, T., Heinonen, A., Sievänen, H., Mikkola, A.: Flexible multibody simulation approach in the analysis of tibial strain during walking. J. Biomech. **41**, 1036–1043 (2008)
5. Allard, P., Cappozzo, A., Lundberg, A., Vaughan, C.L. (eds.): Three-Dimensional Analysis of Human Locomotion. Wiley, Chichester (1998)
6. Anderson, F., Pandy, M.: A dynamic optimization solution for vertical jumping in three dimensions. Comput. Methods Biomech. Biomed. Eng. **2**, 201–231 (1999)
7. Anderson, F., Pandy, M.: Dynamic optimization of human walking. J. Biomech. Eng. **123**, 381–390 (2001)
8. Bessonnet, G., Seguin, P., Sardain, P.: A parametric optimization approach to walking pattern synthesis. Int. J. Robotics Res. **24**(7), 523–536 (2005)
9. Brand, R., Pedersen, D., Friederich, J.: The sensitivity of muscle force predictions to changes in physiologic cross-sectional area. J. Biomech. **19**(8), 589–596 (1986)
10. Cole, G., van den Bogert, A., Herzog, W., Gerritsen, K.: Modeling of force production in skeletal muscle undergoing stretch. J. Biomech. **29**, 1091–1104 (1996)
11. Delp, S., Loan, J.: A graphics-based software system to develop and analyze models of musculoskeletal structures. Comput. Biol. Med. **25**(1), 21–34 (1995)
12. Kim, H., Wang, Q., Rahmatalla, S., Swan, C., Arora, J., Abdel-Malek, K., Assouline, J.: Dynamic motion planning of 3D human locomotion using gradient-based optimization. J. Biomech. Eng. **130**, 03100201–03100214 (2008)
13. Kurz, T., Eberhard, P., Henninger, C., Schiehlen, W.: From Neweul to Neweul-M^2: symbolical equations of motion for multibody system analysis and synthesis. Multib. Syst. Dyn. **24**, 1 (2010)
14. Menegaldo, L., Fleury, A., Weber, H.: Biomechanical modeling and optimal control of human posture. J. Biomech. **36**, 1701–1712 (2003)
15. Menegaldo, L., Fleury, A., Weber, H.: Moment arms and musculotendon lengths estimtion for a three-dimensional lower-limb model. J. Biomech. **37**, 1447–1453 (2004)
16. Nagano, A., Gerritsen, K.: Effects of neuromuscular strength training on vertical jumping performance—a computer simulation study. J. Appl. Biomech. **17**, 113–128 (2001)
17. Pandy, M.: Computer modeling and simulation of human walking. Annu. Rev. Biomed. Eng. **3**, 245–273 (2001)
18. Peasgood, M., McPhee, J., Kubica, E.: Stabilization and energy optimization of a dynamic walking gait simulation. In: Proceedings of the ASME 2005 International Design Engineering Technical Conferences & Computers and Information in Engineering. Long Beach (Sept 24–28 2005)
19. Riener, R., Edrich, T.: Identification of passive elastic joint moments in the lower extremities. J. Biomech. **32**, 539–544 (1999)
20. Rodrgigo, S., Ambrosio, J., Da Silva, M., Penisi, O.: Analysys of human gait based on multibody formulations and optimization tools. Mech. Based Des. Struct Mach. **36**(4), 446–477 (2008)
21. Schiehlen, W.: Multibody system dynamics: roots and perspectives. Multib. Syst. Dyn. **1**, 149–188 (1997)
22. Stein, R., Zehr, E., Lebiedowska, M., Popovic, D., Scheiner, A., Chizeck, H.: Estimating mechanical parameters of leg segments in individuals with and without physical disabilities. IEEE Trans. Rehabil. Eng. **4**(3), 201–211 (1996)
23. Strang, G.: Linear Algebra and Its Applications. 2nd edn. Academic Press, New York (1980)
24. Umberger, B.: Effects of suppressing arm swing on kinematics, kinetics and energetics of human walking. J. Biomech. **41**, 2575–2580 (2008)
25. Umberger, B., Gerritsen, K., Martin, P.: A model of human muscle energy expendidure. Comput. Methods Biomech. Biomed. Eng. **6**(2), 99–111 (2003)
26. van Soest, A., Bobbert, M.: The contribution of muscle properties in the control of explosive movements. Biol. Cybern. **69**, 195–204 (1993)
27. Winter, D.: The Biomechanics and Motor Control of Human Gait: Normal Elderly and Pathological. University of Waterloo Press, Waterloo (1991)
28. Wojtyra, M.: Multibody simulation of human walking. Mech. Based Des. Struct. Mach. **31**(3), 357–379 (2003)
29. Zatsiorsky, V.: Kinematics of Human Motion. Human Kinetics, Champaign, Illinois (1998)